SANDIA REPORT

SAND2013-10779
Unlimited Release
Printed January 2014

MEASUREMENTS OF PROMPT RADIATION-INDUCED CONDUCTIVITY OF PYRALUX®

Fred Hartman, Tom A. Zarick, Michael L. McLain, Tim J. Sheridan, Eric F. Preston and Tom A. Stringer

Prepared by
Sandia National Laboratories
Albuquerque, New Mexico 87185 and Livermore, California 94550

Sandia National Laboratories is a multi-program laboratory managed and operated by Sandia Corporation,
a wholly owned subsidiary of Lockheed Martin Corporation, for the U.S. Department of Energy's
National Nuclear Security Administration under contract DE-AC04-94AL85000.

Issued by Sandia National Laboratories, operated for the United States Department of Energy by Sandia Corporation.

Printed in the United States of America. This report has been reproduced directly from the best available copy.

Available to DOE and DOE contractors from
U.S. Department of Energy
Office of Scientific and Technical Information
P.O. Box 62
Oak Ridge, TN 37831

Telephone:	(865) 576-8401
Facsimile:	(865) 576-5728
E-Mail:	reports@adonis.osti.gov
Online ordering:	http://www.osti.gov/bridge

Available to the public from
U.S. Department of Commerce
National Technical Information Service
5285 Port Royal Rd.
Springfield, VA 22161

Telephone:	(800) 553-6847
Facsimile:	(703) 605-6900
E-Mail:	orders@ntis.fedworld.gov
Online order:	http://www.ntis.gov/help/ordermethods.asp?loc=7-4-0#online

SAND2013-10779
Unlimited Release
Printed January 2014

MEASUREMENTS OF PROMPT RADIATION-INDUCED CONDUCTIVITY OF PYRALUX®

E. F. Hartman, T. A. Zarick, M. L. McLain and T.J. Sheridan
Department, 01343, Radiation Effects Experimentation
Sandia National Laboratories
P. O. Box 5800
Albuquerque, New Mexico 87185-MS 1167

E. F. Preston and T. A. Stringer
ITT Exelis
5009 Centennial Blvd.
Colorado Springs, CO 80919

Abstract

In this report, measurements of the prompt radiation-induced conductivity (RIC) in 3 mil samples of Pyralux® are presented as a function of dose rate, pulse width, and applied bias. The experiments were conducted with the Medusa linear accelerator (LINAC) located at the Little Mountain Test Facility (LMTF) near Ogden, UT. The nominal electron energy for the LINAC is 20 MeV. Prompt conduction current data were obtained for dose rates ranging from ~2 × 10^9 rad(Si)/s to ~1.1 × 10^{11} rad(Si)/s and for nominal pulse widths of 50 ns and 500 ns. At a given dose rate, the applied bias across the samples was stepped between -1500 V and 1500 V. Calculated values of the prompt RIC varied between 1.39×10^{-8} $\Omega^{-1} \cdot m^{-1}$ and 2.67×10^{-7} $\Omega^{-1} \cdot m^{-1}$ and the prompt RIC coefficient varied between 1.25×10^{-18} $\frac{\Omega^{-1} \cdot m^{-1}}{rad/s}$ and 1.93×10^{-17} $\frac{\Omega^{-1} \cdot m^{-1}}{rad/s}$.

ACKNOWLEDGMENTS

The authors would like to acknowledge the support provided by Boeing personnel located at the Little Mountain Test Facility (LMTF) on Hill AFB near Ogden, Utah. Funding for this work was provided by the Radiation Effects and High Energy Density Sciences Program Area.

CONTENTS

FIGURES

TABLES

NOMENCLATURE

DOE	Department of Energy
LINAC	linear accelerator
LMTF	Little Mountain Test Facility
RIC	radiation-induced conductivity

1. INTRODUCTION

Dupont™ Pyralux® is a bonding film that has been vital in the flex circuit industry for decades. [1] The high reliability and insulating properties of the flexible circuit material make it a good candidate for use in complex designs and electronic systems commonly found in military and space applications. In either application, it is likely that the system will be exposed to ionizing radiation at some point during its lifetime. When a dielectric or insulating film is exposed to high-intensity ionizing radiation, it is possible for the electrical conductivity to increase many orders of magnitude due to electron-hole pairs created in the material [1-18]. The free electrons and holes (i.e., excited electrons in the conduction band and holes in the valence band) generated during a radiation exposure lead to a time-dependent increase in the electrical conductivity known as radiation-induced conductivity (RIC). The generated carriers can recombine, become trapped, be swept out of the electrodes, or a combination of the different processes. In highly insulating films such as Pyralux®, the electrons and holes are quickly trapped, but possess some mobility during their lifetime. The RIC is typically characterized by an initial or prompt component (σ_p) that occurs during the radiation pulse and a slow decay following the pulse referred to as the delayed component (σ_d). The total current (I) and electric field are related to the induced conductivity through Ohm's law which can be defined as

$$I = A \cdot \left(\sigma_0 + \sigma_p + \sigma_d\right) \cdot \frac{V_a}{d} + I_{dd}. \tag{1}$$

In (1) A is the exposure area, σ_0 is the dark or static conductivity, V_a is the applied bias, d is the sample thickness, and I_{dd} is the direct drive current produced by the radiation source when the applied bias is zero (i.e., background signal). The delayed conductivity may contain several terms with different decay constants that represent traps of different depths. From (1) it is apparent that the current within the dielectric is dependent on the radiation-induced conductivity and applied bias as well as the attenuation and divergence of the electron beam.

Because an accurate analytical model of the induced conductivity has not yet been established, it is typically necessary to rely on empirical data. One of the reasons for this is that it is difficult to determine the lifetime and mobility of electrons and holes. In polymers, fundamental differences in bonding, morphology, and structure lead to entirely different mechanisms for the transport of electrons [19], [20].

This report summarizes the prompt RIC characteristics of 3 mil (76.2 μm) DuPont™ Pyralux® LF0300 samples. These samples are a sheet adhesive that is a proprietary B-staged modified acrylic adhesive coated on release paper [21]. The experiments on the Pyralux® LF0300 samples were conducted between July 2007 and September 2011 using the Medusa linear accelerator (LINAC) located at the Little Mountain Test Facility (LMTF) near Ogden, UT. Data were obtained as a function of dose rate, pulse width, and applied bias.

[1] DuPont™ and Pyralux® are trademarks or registered trademarks of E.I. du Pont de Nemours and Company.

2. EXPERIMENTAL DETAILS

The Medusa LINAC was used to irradiate 3 mil (76.2 μm) Pyralux® LF0300 samples obtained from DuPont™. The dose rate was varied between ~2 × 10^9 rad(Si)/s to ~1.1 × 10^{11} rad(Si)/s. The dose rates in this report will always be presented in rad(Si)/s to be consistent with industry standards. At a given dose rate, data were obtained for varying pulse widths (50 ns, 100 ns, 200 ns, 500 ns, and 1 μs) and applied biases (-1500 V to 1500 V). Only 50 ns and 500 ns data are shown in this report. Typically, 3-5 shots were taken for every experimental condition to ensure that there was minimal shot-to-shot variation in the response. Prior to the biased experiments, the zero-bias RIC response (i.e., 0 V was applied) was recorded to establish a baseline RIC response for the samples.

When insulating films are irradiated with photons or electrons, stored charge (i.e., space charge) can build up within the sample [5], [14], [17]. The accumulation of fixed trapped space charge will distort the internal field leading to a local space charge effect. The trapped charge effect becomes more severe as the field strength approaches the field created by the externally applied bias. Discharge of the trapped charge after each test condition was accomplished by one or more zero bias irradiations until the recorded current signal matched the initial zero-bias RIC response. In the following sub-sections a brief description of the experimental apparatus and the LINAC is provided. A complete description of the experimental apparatus and procedures is described in [22] and a derivation of the equivalent electrical circuit can be found in [22], [23].

2.1. Experimental Apparatus

The test fixture apparatus includes two separate cells referred to as the upper (URC) and lower RIC cells (LRC). The RIC cell nearest to the electron beam is the URC and the cell below it is the LRC. Figure 1 displays a schematic cross-section of the dielectric samples within the RIC test fixture apparatus. The stacked cells are irradiated concurrently. Each cell consists of a center electrode, two dielectric layers, and ground planes on the outer surface of each dielectric.

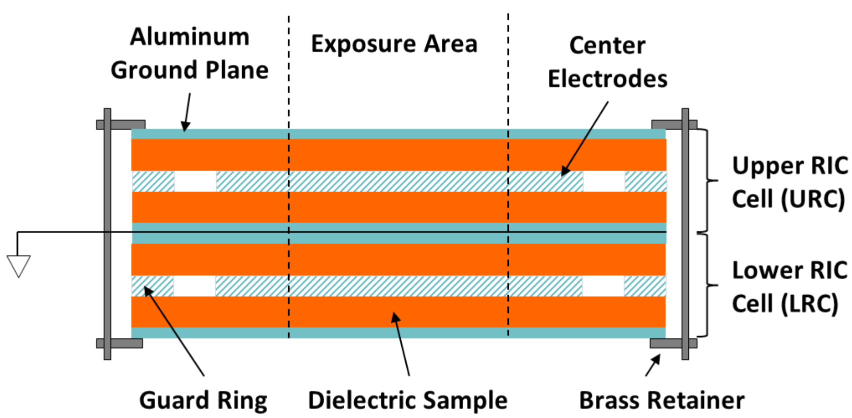

Figure 1. Schematic cross-section of the upper and lower RIC cells within the test fixture apparatus.

The Pyralux® layers are formed from 76.2 μm thick discs, ~2.5 cm in diameter, and are placed on either side of a 30 μm aluminum center electrode. A conductive epoxy was used to combine the center electrodes of the two layers. Two 15 μm aluminum electrodes on the outside of the cell serve as the ground planes. The aluminum guard rings on the outer surface minimize the electric field distortion at the edge of the center electrodes. Bias voltages were applied to the center electrodes and the guard rings. The applied bias on the LRC was equal in magnitude but opposite in polarity to the URC. The RIC cells are designed with two dielectric layers (i.e., one layer above and below a center electrode) to limit the direct drive current during irradiation. In theory, this design will balance the charge lost from the center electrode on each side. However, even when implementing this technique, the direct drive current can still be a substantial part of the total current in materials with a small RIC response. This can make it difficult to discern the contribution of the prompt RIC component.

A typical RIC cell test fixture is pictured in Figure 2. The busses for applying the guard ring voltages (LGR and UGR) and the center electrode biases (URC and LRC) are labeled accordingly. The average cell capacitance of the Pyralux® RIC cells is approximately 474 pF with an average standard deviation of 18 pF. This is for one two-sided cell, either the URC or the LRC. The area of the center electrode is A_{tot} = 5.06 cm^2, but the irradiated area was collimated to ~1.98 cm^2.

Figure 2. A typical RIC cell deisgn.

The test fixture was mounted in a custom chamber that provided vacuum levels between 3 × 10^{-4} and 1 × 10^{-5} torr. A vacuum chamber was necessary to reduce air ionization effects. Radiation entered the test chamber through a collimated aperture that was smaller than the dielectric samples. This assured that only the dielectric was struck by radiation and not the cables or test board. It also guaranteed that the guard rings were not irradiated. All radiation exposures and electrical measurements were performed at room temperature. Figure 3 shows the front side of the test chamber with high voltage cables exiting through vacuum feed-through connectors. The aperture hole in the center of the fixture collimates the LINAC beam. Pictured in Figure 4 is the backside of the vacuum chamber and the front of the Medusa LINAC at the LMTF. A ¼ inch aluminum scatter plate was placed on the front end of the LINAC during these experiments.

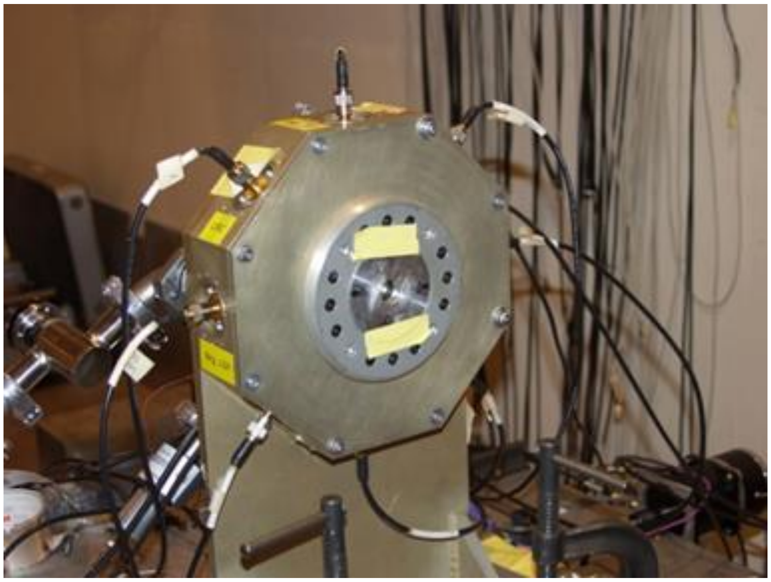

Figure 3. The vacuum experimental chamber with high voltage cables exiting through vacuum feed-through connectors.

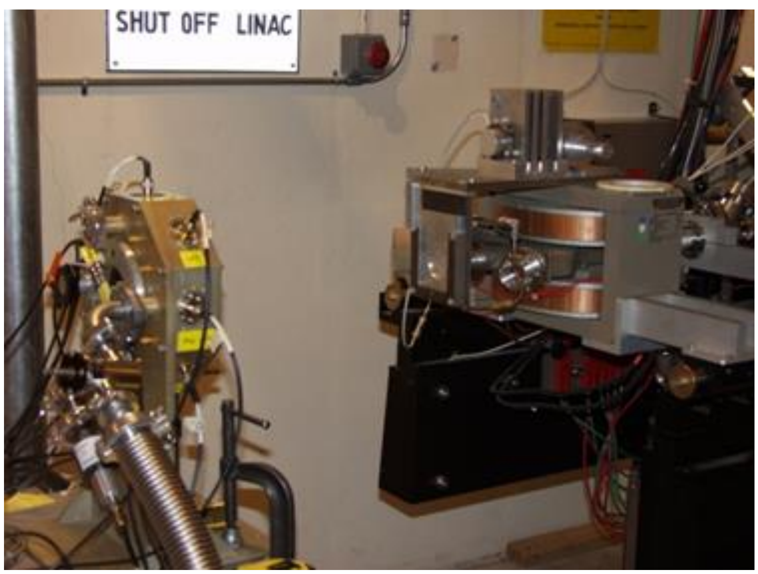

Figure 4. The backside of the vacuum chamber and the front of the Little Mountain Medusa Linear Accelerator at Hill AFB.

2.2. Electron Beam Characteristics

The Medusa LINAC was chosen because it is capable of producing repeatable and predictable radiation output over long periods of time (i.e., reproducible pulsing over a week of experiments). If a radiation source is not capable of providing a consistent output (including the spectrum, pulse width, and fluence), the difficulty of performing repeatable and interpretable experiments is greatly increased. For the electron beam dosimetry, silicon calorimeters were supplemented with thermoluminescent detectors (TLDs), PIN diodes, and photoconductive detectors (PCDs). The dosimetry verified that the machine output for a given setup only varied approximately 1% from shot to shot. Dosimetry was obtained prior to and during the experiments. Measurement accuracy at the LINAC, including dosimetry and recording instruments, is estimated to be about ± 10%.

The LINAC was tuned such that the electron beam current was ~0.8 A over the exposure area. The nominal electron energy for the LINAC is 20 MeV. The range of 20 MeV electrons in in silicon or aluminum (~5 cm) is much greater than the total thickness of the test fixture (~0.7 cm); hence the energy deposition in all four Pyralux® layers is assumed to be nearly uniform. The electron beam differential energy spectrum for the Medusa LINAC is shown in Figure 5. In the figure it can be observed that the average electron kinetic energy for this spectrum is actually 19.2 MeV. It should be noted that the LINAC pulse has a 1.28 GHz microstructure with pulses ~250 ps in duration. However, the microstructure is typically only an issue in extremely fast circuits that are capable of responding to the high-frequency, short duration pulses.

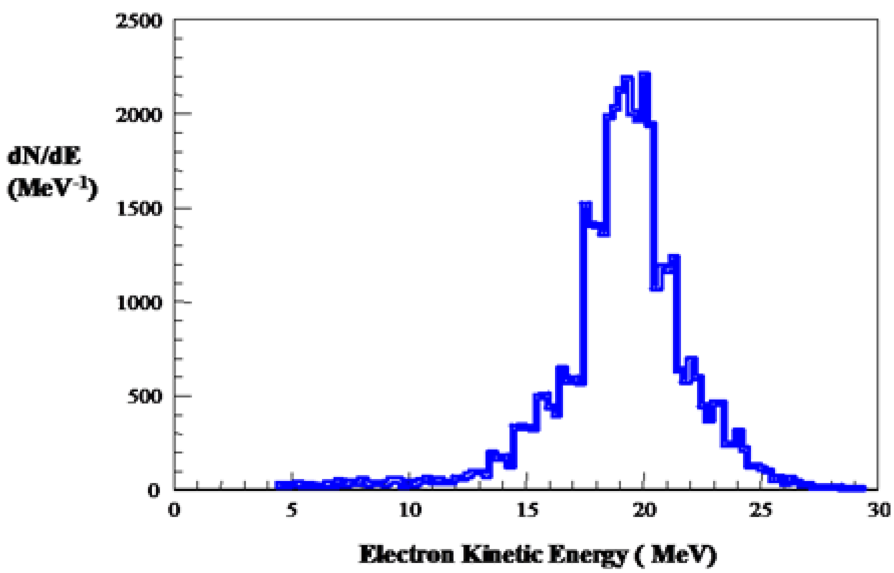

Figure 5. The LINAC electron energy spectrum

3. EXPERIMENTAL RESULTS

DuPont™ Pyralux® products typically consist of a Kapton film with various coatings. However, the samples investigated in these experiments did not contain a Kapton film backing. Recall, these samples are an acrylic adhesive coated on release paper [21]. The experiments involving the Pyralux® samples are summarized in the table below. Note that only the 50 ns and 500 ns data from the 9/2011 experiment will be presented in the report.

Table 1. RIC Experimental Summary

Date	Sample / Series	Shot Numbers	Nominal Dose Rate (rad(Si)/s)	Nominal Pulse Width (ns)
07/2007	PYR2b-1	1198-1210	2.4×10^{9}	500
	PYR2b-2	1211-1223	4.7×10^{9}	500
	PYR2b-3	1224-1236	1.0×10^{10}	500
12/2008	PYR1	2186-2246	1.2×10^{11}	50
	PYR2c	2315-2373	1.1×10^{11}	50
09/2011	PYR6	5347-5504	1.2×10^{10}	50 and 500

3.1. PYR2b

The PYR2b test series (i.e., 2b-1, 2b-2, and 2b-3) was performed in June 2007. The nominal dose rate was varied from 2.4×10^{9} rad(Si)/s to 1.0×10^{10} rad(Si)/s and the radiation pulse width was 500 ns (refer to Table 1). Representative plots of the zero-bias and biased shots from the 2b-1 experiments are shown in Figure 6 and Figure 7, respectively. All RIC signals were smoothed using a 65-point Savitzky-Golay filter. During each measurement, a diamond PCD was used to determine the shape of the beam pulse. In the plots, the PCD signal has been rescaled to have approximately the same magnitude as the RIC signals. The figures reveal that the direct drive signal is positive for both the URC and the LRC and that the peak values for the biased shots are approximately 2× larger than the zero-bias shots. Note that the RIC signal is positive for a negatively applied bias and vice versa. Also observe that both the URC and LRC response have approximately the same magnitude. Recall from (1) that the total current is the summation of the RIC current plus the direct drive current. Thus, one would expect the positively biased cell to have less net current because the resulting polarity of the signal is opposite the direct drive current. However, it appears that the biased response lacks the direct drive component.

The plots in Figure 8 and Figure 9 are the zero-bias and biased shots from the 2b-2 test series and Figure 10 and Figure 11 are plots from the 2b-3 test series. Similar to the 2b-1 experiments, the biased shots are approximately 2× greater than the zero-bias LRC response and the direct drive component does not seem to impact the overall response. Also note that the direct drive component for the URC is negligible in comparison to the LRC for the 2b-3 experiments and half the value in the 2b-2 experiments. This response is not well understood. The measured RIC signals for 2b-3 are approximately 4× greater than the RIC signals for 2b-1 due to the ~4× higher dose rate (and 2× greater than the RIC signals for 2b-2). The observed rise-time characteristics and the post-pulse decay are typical features of all biased shots.

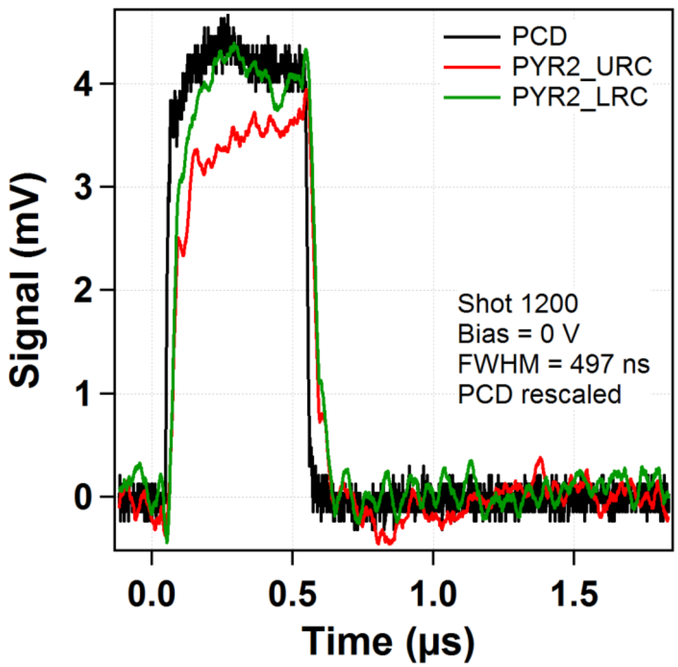

Figure 6. Representative plot of the measured RIC signals versus time for an applied bias of 0 V. These data were obtained from the PYR2b-1 test series and for a dose rate of ~2.4 × 10^9 rad(Si)/s.

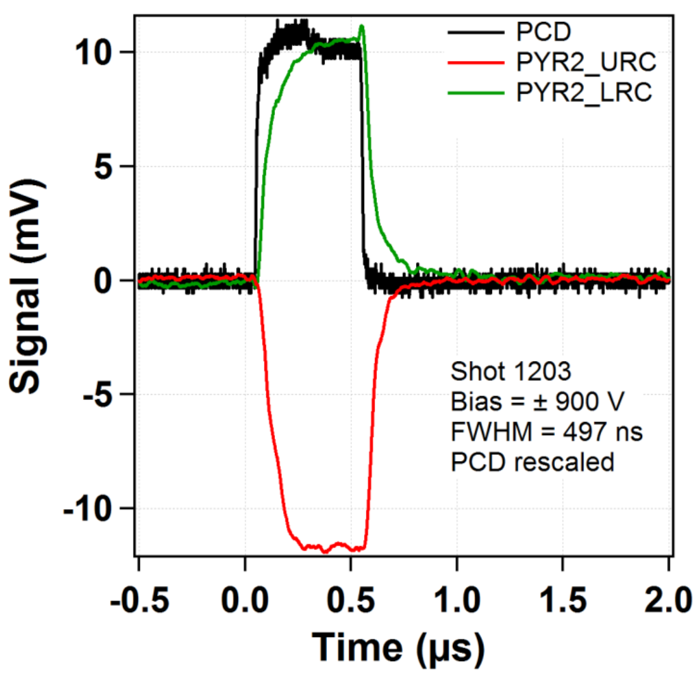

Figure 7. Representative plot of the measured RIC signals versus time from the PYR2b-1 test series. These data were obtained for a dose rate of ~2.4 × 10^9 rad(Si)/s, FWHM of ~497 ns, and applied bias of ± 900 V depending on the cell.

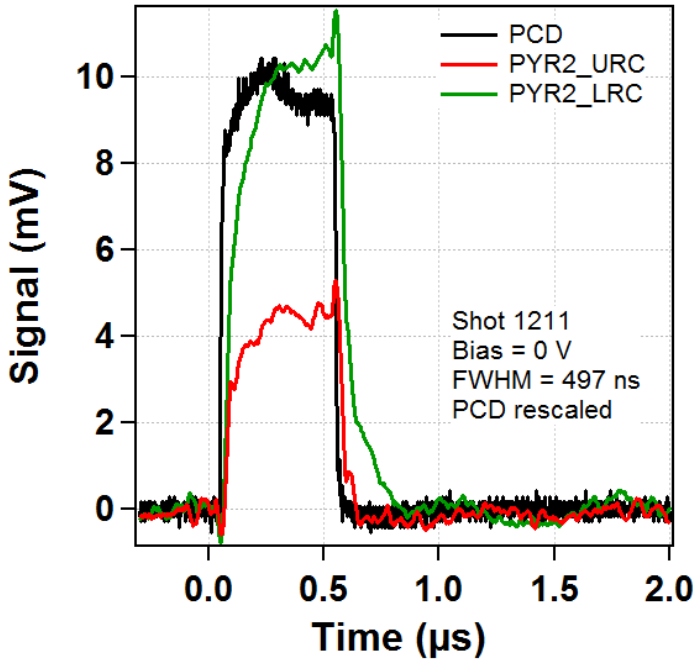

Figure 8. Representative plot of the measured RIC signals versus time for an applied bias of 0 V. These data were obtained from the PYR2b-2 test series and for a dose rate of ~4.7 × 10^9 rad(Si)/s.

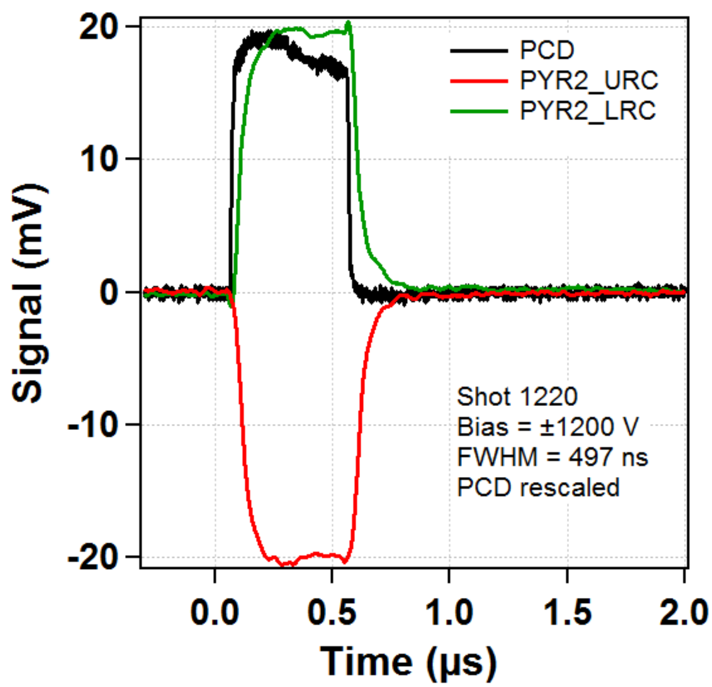

Figure 9. Representative plot of the measured RIC signals versus time from the PYR2b-2 test series. These data were obtained for a dose rate of ~4.7 × 10^9 rad(Si)/s, FWHM of ~497 ns, and applied bias of ± 1200 V depending on the cell.

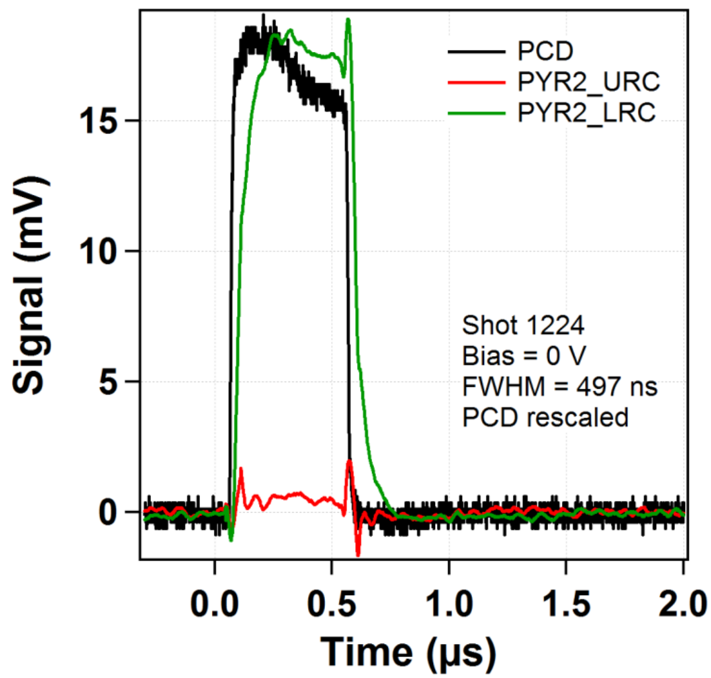

Figure 10. Representative plot of the measured RIC signals versus time for an applied bias of 0 V. These data were obtained from the PYR2b-3 test series and for a dose rate of ~1 $\times$ 10^{10} rad(Si)/s.

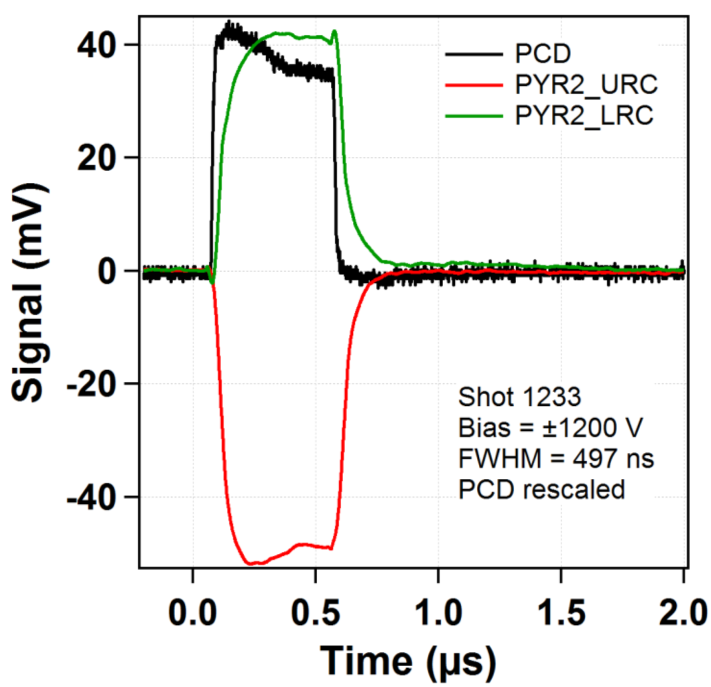

Figure 11. Representative plot of the measured RIC signals versus time from the PYR2b-3 test series. These data were obtained for a dose rate of ~1 $\times$ 10^{10} rad(Si)/s, FWHM of ~497 ns, and applied bias of ± 1200 V depending on the cell.

Shown in Figure 12 is a plot of the measured voltage (V_M) versus applied bias (V_a) with fits for the 2B-1 series. The data were obtained from the URC RIC signals only. The plots for 2b-2 and 2b-3 had similar characteristics. Here, the measured voltage is obtained by integrating the RIC signal and then dividing by the full width half max (FWHM) of the response (i.e., average of the prompt RIC signal). The peak RIC signal can be used instead of the average RIC signal; however the average RIC signal is usually more representative of the current increase during a pulsed exposure. Furthermore, the peak RIC signal may not account for the direct drive current and may be dominated by the delayed RIC.

As observed in the data, a positive applied bias resulted in a different y-intercept (i.e., measured voltage at an applied bias 0) and a steeper slope than a negative applied bias. The negative value of the y-intercept is indicative of the lack of a direct drive component (refer to Figure 6). Because the zero bias data matches well with the negative bias shots, only the negative bias slope is used to determine the conductivity and RIC coefficient.

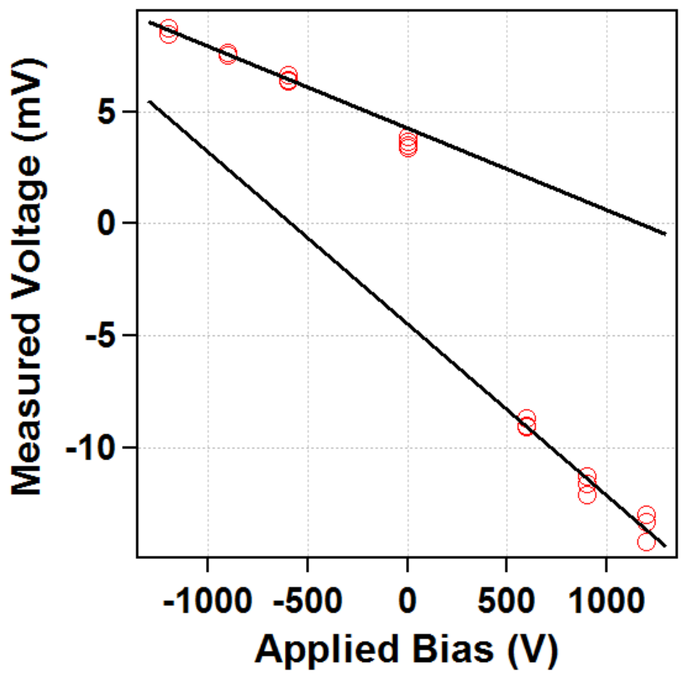

Figure 12. Plot of the measured voltage versus applied bias for the URC of series 2b-1. These data points were obtained for a dose rate of ~2.4 × 10^9 rad(Si)/s and a pulse width of ~500 ns.

3.2. PYR1 and PYR2c

The PYR1 and PYR2c test series was performed in December 2008. The nominal dose rate in these experiments was 10^{11} rad(Si)/s and the radiation pulse width was ~35 ns. Representative plots of the zero-bias and biased shots for the PYR1 test series are provided in Figure 13 and Figure 14, respectively. Plots from the PYR2c test series are shown in Figure 15 and Figure 16. These experiments were performed with a radiation pulse width of ~35 ns. The zero-bias shots (Figure 13 and Figure 15) are almost identical for the URC and LRC. Also notice that the signals are not reaching equilibrium by the end of the radiation pulse. The negative dip that occurs at the beginning of the radiation pulse is present on all signals (including the wider pulse width data). However, the magnitude of the negative dip varies and is sometimes small compared to the signal voltage (as seen in the wider pulse width zero-bias shots above). One possible cause of the negative dip is a knock-off current due to the emission of electrons off the surface of the center electrode into the dielectric. This current will quickly neutralize due to local fields. The remaining signal is then a direct drive, knock-on current from the attenuation of the electron beam.

Unlike the data discussed in the previous subsection, the biased shots from the PYR1 and PYR2c test series exhibit the expected asymmetry between the LRC and the URC response. In fact, the biased shot signals are being dominated by the direct drive response (Figure 14 and Figure 16). For example, when the bias on the cell is positive (e.g., URC data in the figures), the response is much smaller because the resulting polarity of the RIC signal is opposite the direct drive current. When the bias on the cell is negative, the peak responses are only slightly greater than the zero-bias signals (LRC data). It is also evident from the data that there is a significant delayed RIC component. A similar type of response was observed for the other biased shots in this test series. Because the direct drive current was a substantial part of the total, it was difficult to discern the contribution of the prompt RIC component.

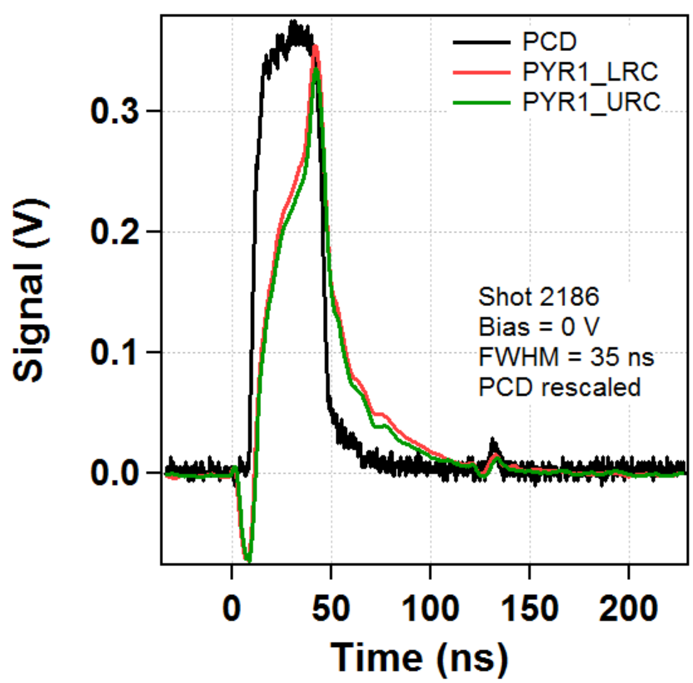

Figure 13. Representative plot of the measured RIC signals versus time for an applied bias of 0 V. These data were obtained from the PYR1 test series and for a dose rate of ~1.1 × 10^{11} rad(Si)/s.

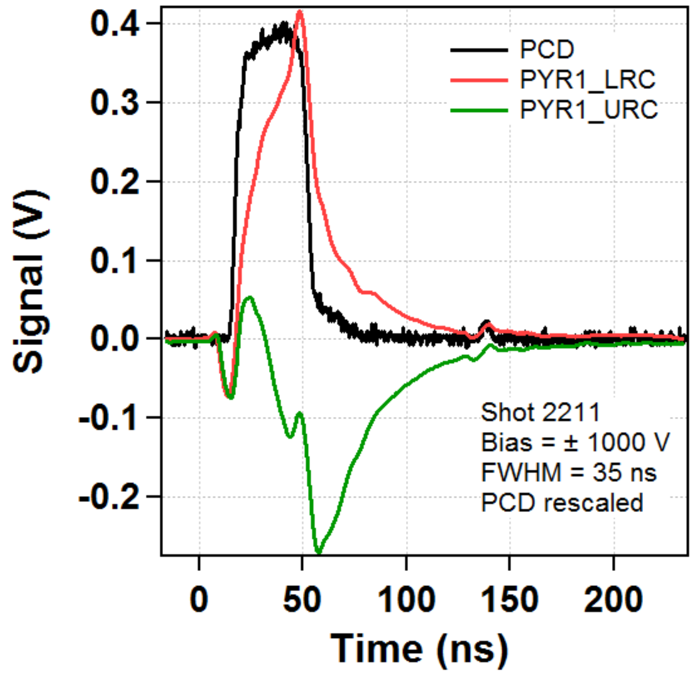

Figure 14. Representative plot of the measured RIC signals versus time from the PYR1 test series. These data were obtained for a dose rate of ~1.1 × 10^{11} rad(Si)/s, FWHM of ~35 ns, and applied bias of ± 1000 V depending on the cell.

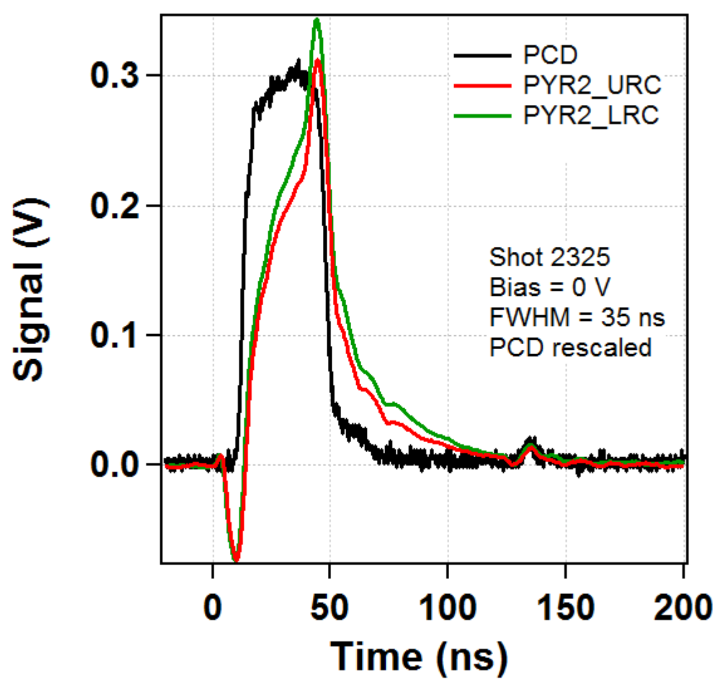

Figure 15. Representative plot of the measured RIC signals versus time for an applied bias of 0 V. These data were obtained from the PYR2c test series for a dose rate of ~1.1 × 10^{11} rad(Si)/s.

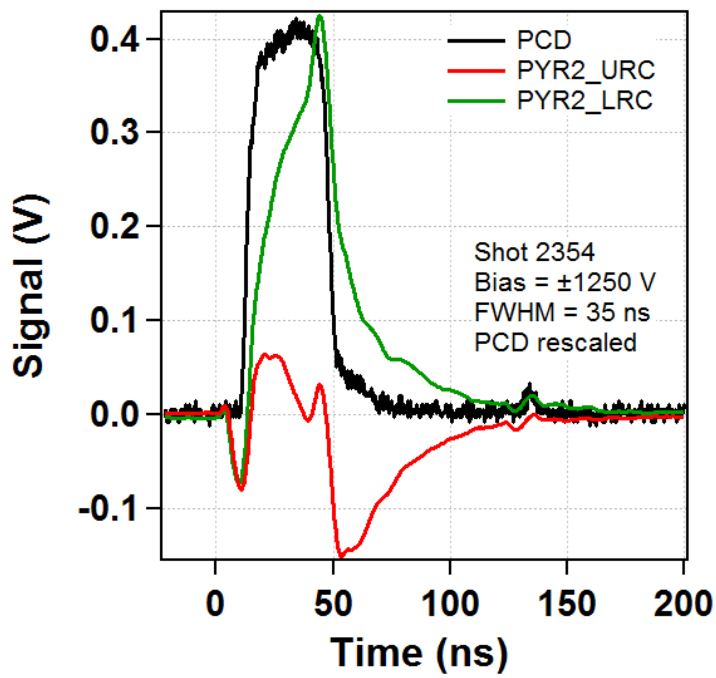

Figure 16. Representative plot of the measured RIC signals versus time from the PYR2c test series. These data were obtained for a dose rate of ~1.2 × 10^{11} rad(Si)/s, FWHM of ~35 ns, and applied bias of ± 1250 V depending on the cell.

Shown in Figure 17 is a plot of V_m versus V_a with fits for the PYR2c series. The data were obtained from the URC. PYR1 had similar characteristics, but more variation was observed between shots for identical experimental conditions. In Figure 17, the measured voltage is obtained by integrating the RIC signal and then dividing by the FWHM of the response (i.e., average of the prompt RIC signal). However, each signal begins with a small negative dip and then has a significant delayed component following the end of the radiation pulse. To ensure that only the prompt RIC component is used in calculating the measured voltage, only the signal that occurs during the radiation pulse was integrated. As observed in the data, a positive applied bias again resulted in a different y-intercept and a steeper slope than a negative applied bias. The difference in slopes may be due to field-enhanced conductivity. When there is positive bias, the charge deposited in the dielectric (near the electrodes) will generate an electric field which assists the tunneling of carriers from traps thereby increasing the conductivity. This may also be thought of as effectively decreasing the thickness of the dielectric. Also notice that the fits to the negative bias shots and the positive bias shots did not align with the zero bias data (although the negative bias data is much closer).

Another technique that can be implemented to determine the measured RIC voltage is to take the peak value 90% into the pulse, as determined by the FWHM. This avoids taking into account the noise, negative spikes, and delayed component. A plot of the measured voltage versus applied bias as determined by the 90% technique is shown in Figure 18. As seen in the data, there is less variation for equivalent shots and the negative bias shots are now better aligned with the zero bias shots. This technique resulted in slight changes in the calculated slopes. Because the data suggest that this technique is more accurate for shorter pulse widths, this technique was used to calculate the conductivity (for both PYR1 and PYR2c).

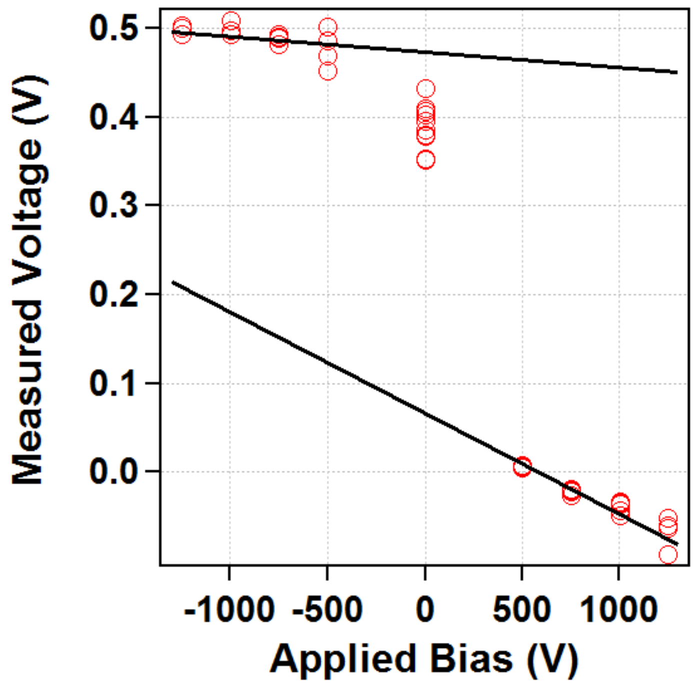

Figure 17. Plot of the URC measured voltage versus applied bias for the PYR2c test series. These data points were obtained for a dose rate of ~1.1 $\times$ 10^{11} rad(Si)/s and a pulse width of ~35 ns.

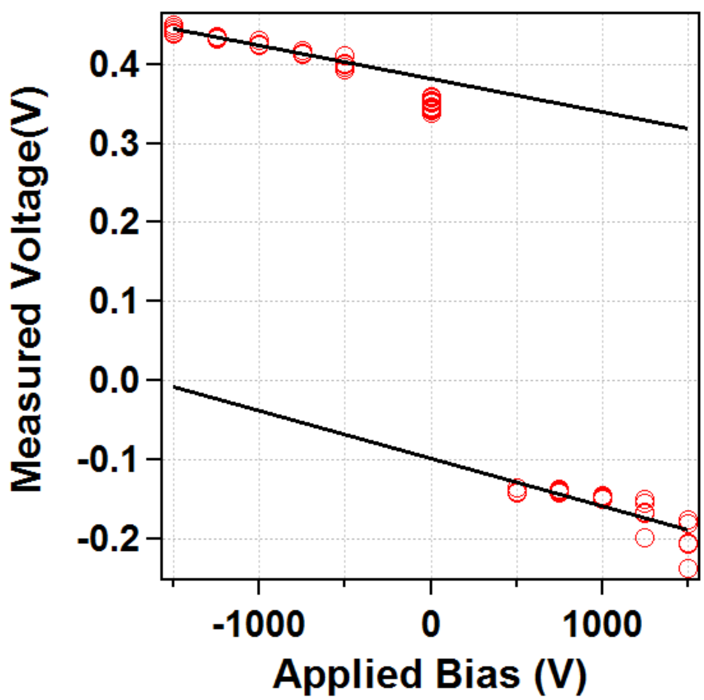

Figure 18. Plot of the URC measured voltage versus applied bias for the PYR2c test series. The measured voltage was determined using the 90% method.

3.3. PYR6

The PYR6 test series was performed in September 2011. Data were obtained for nominal pulse widths of 50 ns, 100 ns, 200 ns, 500 ns, and 1 µs. The dose rate was held constant at approximately 10^{10} rad(Si)/s. Data were also obtained for a 1 µs pulse width and a dose rate of 10^9 rad(Si)/s. During the exposures, bias voltages of 0 V, ± 200 V, ± 400 V and ± 600 V were applied to the Pyralux samples. After each biased experiment, 5 clearing shots were taken to eliminate any stored charge in the sample. It was assumed that once the response matched the original 0 V baseline RIC response, all stored charge had been removed from the cells. Three shots were taken at each test condition. Minimal shot-to-shot variation was seen in the results. In this report, only the results for a dose rate of 10^{10} rad(Si)/s and nominal pulse widths of 50 ns and 500 ns are provided.

Representative plots of the zero-bias shots for a radiation pulse width of 500 ns and 60 ns are shown in Figure 19 and Figure 20, respectively. Note that the direct drive in the URC is much less than in the LRC in each case. This is not well understood. The negative dip that occurs at the beginning of the radiation pulse and the spike at the end of the pulse exist on all signals. However, the beam pulse does not have the anomalous spikes at the beginning and end of the pulse. As discussed above, it is has been hypothesized that the spikes in the RIC response are due to charge being knocked off the center electrode at the beginning of the pulse and then re-deposited on the electrode at the end of the pulse.

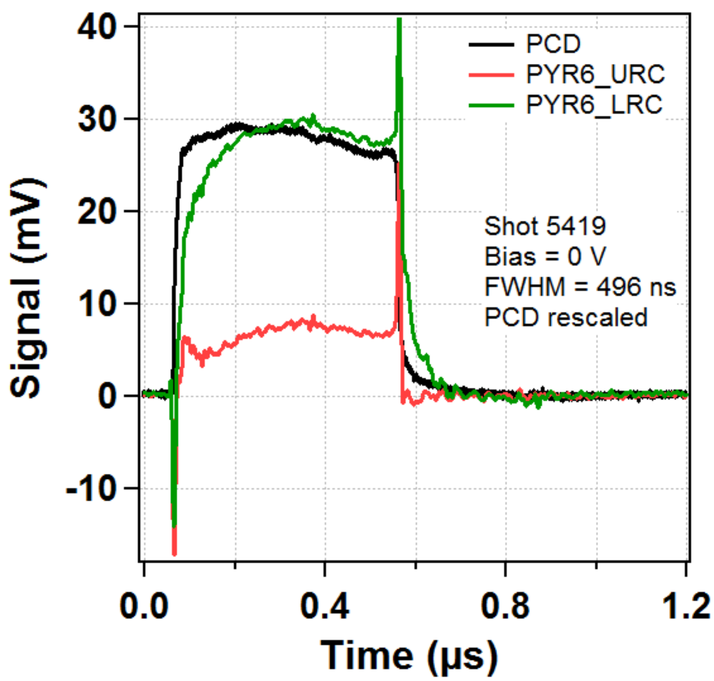

Figure 19. Representative plot of the measured RIC signals versus time from the PYR6 test series. These data were obtained for a dose rate of ~1 × 10^{10} rad(Si)/s, a nominal radiation pulse width of 500 ns, and an applied bias of 0 V.

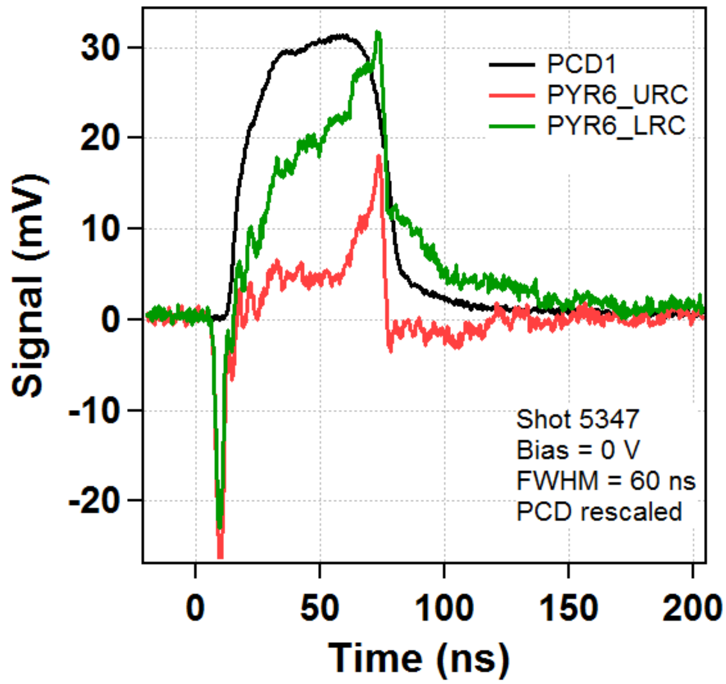

Figure 20. Representative plot of the measured RIC signals versus time from the PYR6 test series. These data were obtained for a dose rate of ~1 × 10^{10} rad(Si)/s, a radiation pulse width of 60 ns, and an applied bias of 0 V.

Presented in Figure 21 and Figure 22 are representative RIC signals versus time for the URC and the LRC when a bias is applied. In this data, the applied bias was ± 600 V, the dose rate was 1.2 x 10^{10} rad(Si)/s and the pulse width was either 60 ns or 500 ns. As expected, the RIC signals are opposite in polarity of the applied bias. However, as with the other samples, the biased shots do not exhibit the asymmetry that one would expect when the magnitude of the direct drive component is comparable to the magnitude of the RIC signals. That is, when the RIC signal is positive (negative applied bias) and the same polarity as the direct drive, the two signals should be additive. When the RIC signal is negative (positive applied bias) and the opposite polarity of the direct drive, the two signals should subtract. From this logic, the magnitude of the RIC signal should be higher when the applied bias is negative and near zero or even slightly positive when the applied bias is positive. As seen in the data this is not the case. It is also apparent that the 60 ns biased data is dominated by the direct drive when the applied bias is negative.

Shown in Figure 23 are plots of the V_M versus V_a for a pulse width of 60 ns and 500 ns, respectively. The dose rate was 1.2 x 10^{10} rad(Si)/s. The measured voltage for the 500 ns case was obtained by integrating the RIC signal and then multiplying by the full width half max (FWHM) of the response. Similar to the other short pulse width calculations, the measured voltage for the 60 ns case was calculated using the 90% technique discussed in the previous section. Determining the appropriate technique to calculate the measured voltage is vital given that the slope of V_M versus V_a is used to estimate the radiation-induced conductivity.

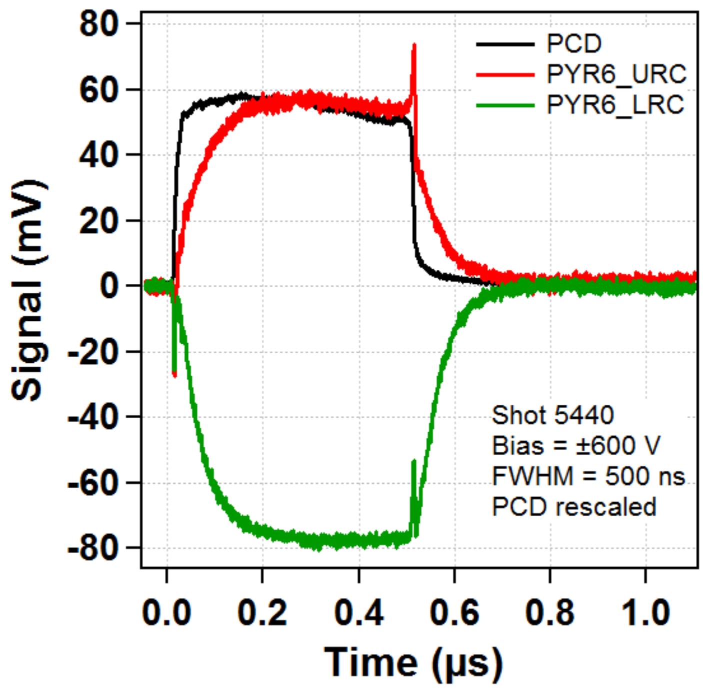

Figure 21. Representative plot of the measured RIC signals versus time for PYR6. These data were obtained for a dose rate of ~1.2 × 10^{10} rad(Si)/s, FWHM of ~500 ns, and applied bias of ± 600 V depending on the cell.

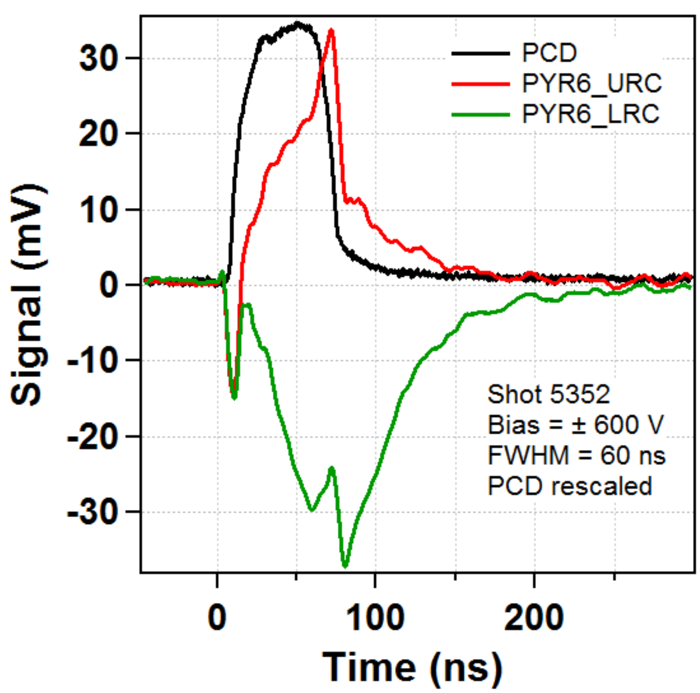

Figure 22. Representative plot of the measured RIC signals versus time for PYR6. These data were obtained for a dose rate of ~1.2 × 10^{10} rad(Si)/s, FWHM of ~60 ns, and applied bias of ± 600 V depending on the cell.

Similar to the PYR2c and PYR1 short pulse width data, these signals are almost entirely direct drive. This makes it difficult to calculate the measured voltage. With respect to the 500 ns data, it is difficult to accurately calculate the RIC because the maximum applied bias was ±600 V. In the other experiments, this was typically the minimum voltage. For an applied bias less than 600 V, the measured voltage is dominated by a direct drive component. It is also interesting to note that the direct drive in this experiment was approximately 2× higher than it was when testing sample 2B-3 in a similar experiment.

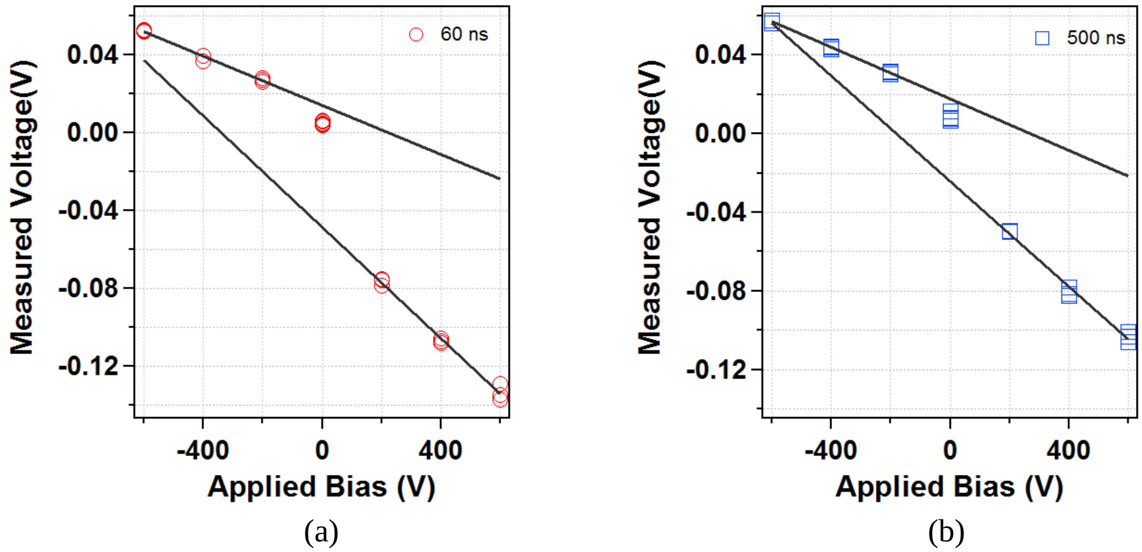

Figure 23. Plot of the URC measured voltage versus applied bias for a radiation pulse width of (a) 60 ns and (b) 500 ns. These data points are from the PYR6 test series and were obtained for a dose rate of ~1.2 × 10^{10} rad(Si)/s.

4. DISCUSSION

The prompt conductivity (i.e., RIC) can be calculated directly from (1) or through the preferred slope method described in [5], [17] and later refined in [22]. The resulting equation for the prompt conductivity is

$$\sigma_p = \frac{d}{2AR_s}\frac{m}{m-1} \tag{2}$$

where m is the slope of the V_M versus V_a plot, R_s is the scope resistance (50 Ω), and A is the exposure area. As discussed previously, the measured voltage is typically obtained by integrating the RIC signal and then dividing by the full width half max (FWHM) of the response (i.e., average of the prompt RIC signal). The peak RIC signal (or the value 90% into signal) can be used instead of the average RIC signal; however the average RIC signal is usually more representative of the current increase during a pulsed exposure. Despite this, it was apparent in the shorter pulse width data that using the 90% technique to determine the measured voltage was the most accurate.

The dose rate dependence of prompt RIC in amorphous solids is often modeled as [5], [7], [17]

$$\sigma_p(\dot{D}) = k_c\dot{D}^{\Delta} \tag{3}$$

where $\dot{D}$ is the dose rate, k_c is a constant RIC coefficient in units of $\left[\frac{\Omega^{-1}m^{-1}}{rad/s}\right]$, and Δ is an experimentally determined parameter. In the slope method, it is typically assumed that the RIC coefficient absorbs all dependencies of the experimental parameters. In other words, $\sigma_p = k(\dot{D}, E, \ldots) \cdot \dot{D}$ where E is the electric field. For a narrow range of dose rates, the conductivity is presumed to be nearly linear and the RIC coefficient can be defined as

$$k_c = \frac{1}{\dot{D}}\frac{d}{2AR_s}\frac{m}{m-1} \tag{4}$$

The assumption is that $k\dot{D}$ varies slowly enough to make the linear approximation locally valid.

The calculated values for the prompt RIC and the RIC coefficient are shown in Table 2. All calculations were made using the data obtained when the applied bias was negative. The values for these parameters are comparable to previous results on Pyralux and other materials [5], [22], [24], [25]. However, as with the previous experiments, there are occasional anomalies in the RIC response characteristics that are not well understood at this time. This includes spikes at the beginning and end of the RIC signals that are not seen in the beam wave shape, no apparent direct drive impact on the RIC response characteristics, and the slope difference between the positive and negative data on the measured voltage versus applied bias plots. These issues complicate the calculation of the RIC and the RIC coefficient.

Also provided in the table is the standard regression error as determined from the linear fits on the V_M versus V_a plots. The standard error measures the accuracy of the predicted values to the measured values. Recall that the regression line is the line that minimizes the sum of squared deviations of prediction (also called the sum of squares error). The standard error of the estimate can be written as

$$\sigma_{est} = \sqrt{\frac{\sum(Y-Y')^2}{N}} \tag{5}$$

where σ_{est} is the standard error of the estimate, Y is the measured value from the experiment, Y' is the predicted value, and N is the number measurements. The numerator is the sum of squared differences between the measured values and the predicted values.

Table 2. Calculated Values of the RIC and RIC Coefficient

Series	Cell	Pulse width (ns)	Dose rate (rad(Si)/s)	σ_p (Ω^{-1} m^{-1})	σ_{est}	k_c (Ω^{-1} m^{-1}/rad/s)
PYR2b-1	URC	500	2.13×10^{9}	1.39×10^{-8}	0.007	6.91×10^{-18}
PYR2b-1	LRC	500	2.13×10^{9}	1.39×10^{-8}	0.011	7.70×10^{-18}
PYR2b-2	URC	500	4.15×10^{9}	3.37×10^{-8}	0.008	6.69×10^{-18}
PYR2b-2	LRC	500	4.15×10^{9}	2.18×10^{-8}	0.016	4.23×10^{-18}
PYR2b-3	URC	500	8.84×10^{9}	5.80×10^{-8}	0.019	6.38×10^{-18}
PYR2b-3	LRC	500	8.84×10^{9}	5.90×10^{-8}	0.028	6.25×10^{-18}
PYR2c	URC	35	1.1×10^{11}	1.61×10^{-7}	0.319	1.38×10^{-18}
PYR2c	LRC	35	1.1×10^{11}	1.93×10^{-7}	0.312	1.62×10^{-18}
PYR1	URC	35	1.1×10^{11}	1.56×10^{-7}	0.386	1.42×10^{-18}
PYR1	LRC	35	1.1×10^{11}	1.50×10^{-8}	0.340	1.25×10^{-18}
PYR6	URC	60	1.16×10^{10}	2.03×10^{-7}	0.056	1.46×10^{-17}
PYR6	LRC	60	1.16×10^{10}	1.58×10^{-7}	0.054	1.35×10^{-17}
PYR6	URC	500	1.24×10^{10}	2.67×10^{-7}	0.043	1.93×10^{-17}
PYR6	LRC	500	1.24×10^{10}	2.42×10^{-7}	0.043	1.81×10^{-17}

Shown in Figure 24 and Figure 25 are plots of the radiation-induced conductivity versus dose rate. The conductivities were calculated using (2). The fit is only for the PYR2b test series (the 35 ns data and the PYR6 data were omitted). The lines above and below the power-law fit in Figure 24 represent the 95.4% confidence interval bounds. Indeed all data points fall within this confidence interval except for the PYR6 test series. Two possible reasons that PYR6 data is not within the bounds are that the maximum applied bias during the PYR6 test series was only 600 V. This likely impacted the calculation of the slope on the V_M versus V_a plot because lower bias data is typically dominated by direct drive. In the other experiments the lowest bias was typically around 600 V. Another issue that was observed in this data was the direct drive component was twice as large when compared to an equivalent experiment on the PYR2b samples. In Figure 25, error bars are provided which represent the standard regression error. As seen in the plot, these values are minimal for most of the data points.

Despite anomalies in the data, the data are fairly consistent across the series and yield a reasonable fit for conductivity in the PYR2b test series (Figure 24). The power-law fit for the conductivity is

$$\sigma(\dot{D}) = 6.87 \times 10^{-18} \dot{D}^{0.998}. \tag{6}$$

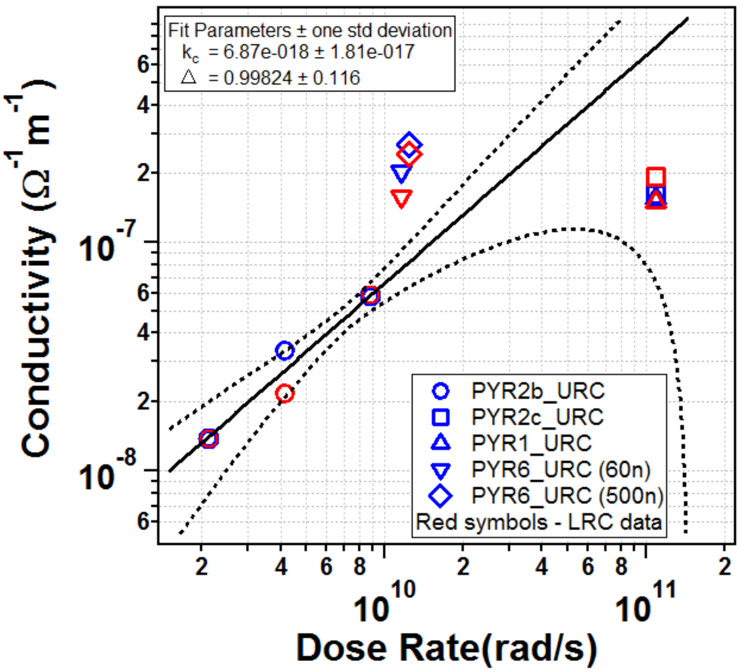

Figure 24. Plot of the radiation-induced conductivity versus dose rate for several different Pyralux films (refer to Table 2). The fit is only for the PYR2b URC samples series. The dashed lines represent the 95.4% confidence interval bounds.

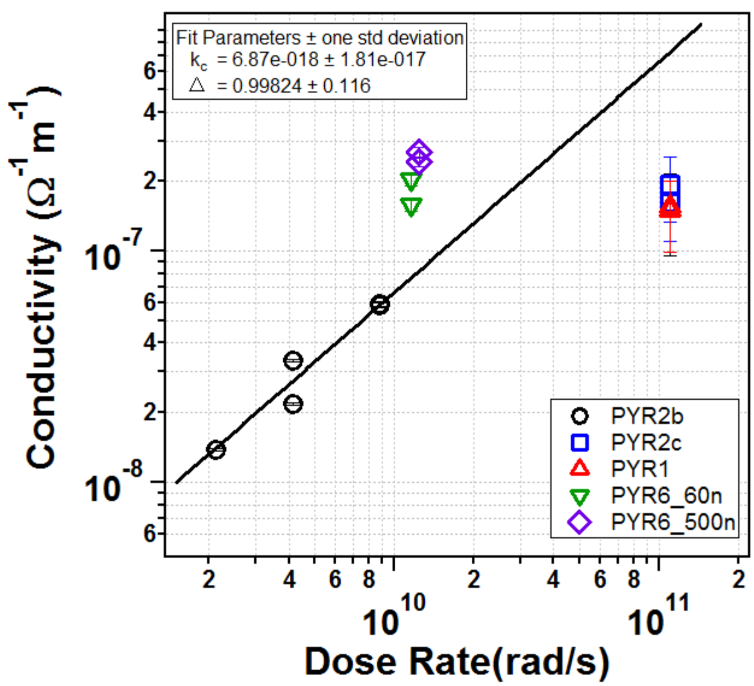

Figure 25. Plot of the radiation-induced conductivity versus dose rate for several different Pyralux films (refer to Table 2). The fit is only for the PYR2b samples series. The error bars represent the standard regression error calculated from the V_m versus V_b plots.

Shown in Figure 26 is a plot of the RIC coefficient versus dose rate. The RIC coefficient was calculated using (4). Because the PYR6 test series resulted in higher conductivity values than expected, this data was not included in this plot. As seen in the data, there is a downward trend in the RIC coefficient as the dose rate increases.

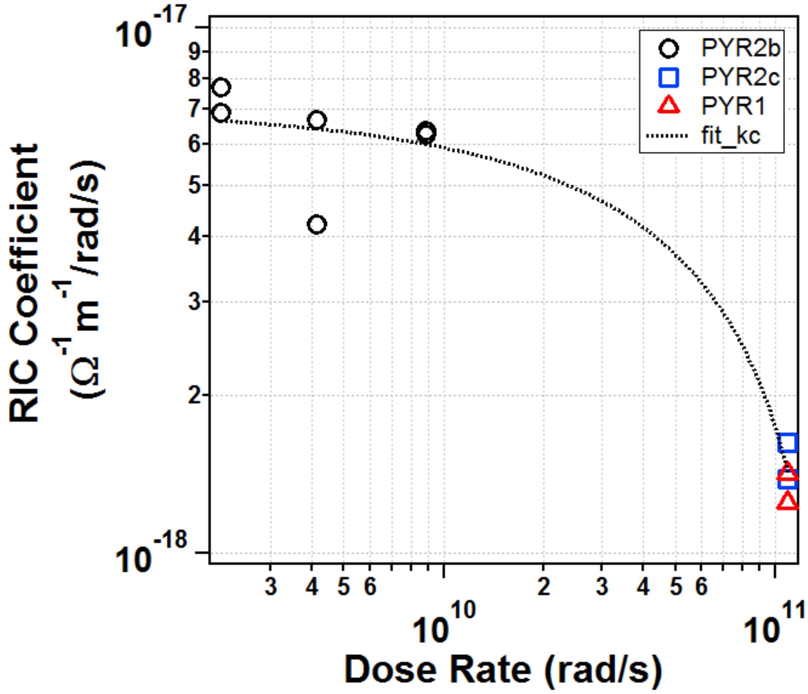

Figure 26. Plot of the RIC coefficient versus dose rate for several different Pyralux films. The PYR6 data is not shown (refer to Table 2). The trend for PYR2b, PYR2c, and PYR1 is downward for increasing dose rates.

5. SUMMARY

In this report, measurements of the prompt radiation-induced conductivity (RIC) in 3 mil samples of Pyralux® were presented as a function of dose rate, pulse width, and applied bias. The experiments were conducted with the Medusa linear accelerator (LINAC) located at the Little Mountain Test Facility (LMTF) near Ogden, UT. Prompt radiation-induced conductivity data were obtained for dose rates ranging from ~2×10^9 rad(Si)/s to ~1.1×10^{11} rad(Si)/s and for nominal pulse widths of 50 ns and 500 ns. At a given dose rate, the applied bias across the samples was stepped between -1500 V and 1500 V.

All calculations were made using the data obtained when the applied bias was negative. The RIC values are comparable to previous results, but as with the previous experiments, there are anomalies in the RIC response characteristics that are not well understood at this time. This includes spikes at the beginning and end of the RIC signals that are not seen in the beam wave shape, no apparent direct drive impact on the RIC response characteristics, and the slope difference between the positive and negative data on the measured voltage versus applied bias plots. Furthermore, the shorter pulse width data was dominated by the direct drive component and was not reaching an equilibrium state before the end of the pulse. Calculated values of the prompt RIC varied between 1.39×10^{-8} $\Omega^{-1} \cdot m^{-1}$ and 2.67×10^{-7} $\Omega^{-1} \cdot m^{-1}$ and the prompt RIC coefficient varied between 1.25×10^{-18} $\frac{\Omega^{-1} \cdot m^{-1}}{rad/s}$ and 1.93×10^{-17} $\frac{\Omega^{-1} \cdot m^{-1}}{rad/s}$. Overall, the values for the RIC and RIC coefficient in Pyralux are small compared to other dielectrics.

.

6. REFERENCES

[1] J. F. Fowler, "X-ray induced conductivity in insulating materials," *Proc. Roy. Soc. London. Series A, Math. and Phys. Sci.,* vol. 236, no. 1207, pp. 464-480, Sept. 1956.

[2] R. C. Weingart, R. H. Barlett, R. S. Lee, and W. Hofer, "X-ray-induced photoconductivity in dielectric films," *IEEE Trans. Nucl. Sci.,* vol. NS-19, no. 6, pp. 15-22, Dec. 1972.

[3] T. J. Ahrens and F. Wooten, "Electrical conductivity induced in insulators by pulsed radiation," *IEEE Trans. Nucl. Sci.,* vol. NS-23, no. 3, pp. 1268-1272, Jun. 1976.

[4] R. C. Hughes, "Radiation-induced conductivity in polymers: Poly-N-Vinylcarbazole," *IEEE Trans. Nucl. Sci.,* vol. 18, no. 6, pp. 281-287, Dec. 1971.

[5] S. H. Face, C. A. Eklund, and T. A. Stringer, "Measurement of radiation induced conductivity for hardened cable dielectric materials at high fluence," *IEEE Trans. Nucl. Sci.,* vol. NS-30, no. 6, pp. 4450-4456, Dec. 1983.

[6] D. K. Nichols and V. A. J. van Lint, "Theory of transient electrical effects in irradiated insulators," *IEEE Trans. Nucl. Sci.,* vol. 13, no. 6, pp. 119-126, Dec. 1966.

[7] D. L. Shaeffer and J. M. Siegel, "Analysis of time-dependent radiation-induced conductivity in dielectrics and effect on cable SGEMP," *IEEE Trans. Nucl. Sci.,* vol. NS-29, no. 6, pp. 1745-1753, Dec. 1982.

[8] R. C. Hughes, "Transient x-Ray induced conductivity in single crystal and fused quartz," in *27th Annual Symposium on Frequency Control*, 1973, pp. 118-119.

[9] R. C. Hughes, "Electronic and ionic charge carriers in irradiated single crystal and fused quartz," *Radiation Effects,* vol. 26, no. 4, pp. 225-235, Apr. 1975.

[10] R. C. Hughes, "Generation, transport, and trapping of excess charge carriers in Czochralski-grown sapphire," *Phys. Rev. B,* vol. 19, no. 10, pp. 5318-5328, May 1979.

[11] S. R. Kurtz, C. Arnold, and R. C. Hughes, "The development of a radiation hardened polymer dielectric by chemical doping," *IEEE Trans. Nucl. Sci.,* vol. 30, no. 6, pp. 4077-4080, Dec. 1983.

[12] L. W. Parker and A. Meulenberg, "Theory of radiation-induced and carrier-enhanced conductivity: space charge and contact effects," *IEEE Trans. Nucl. Sci.,* vol. 31, no. 6, pp. 1368-1374, Dec. 1984.

[13] J. F. Fowler, "Radiation-induced conductivity in the solid state, and some applications," *Phys. Med. Biol.,* vol. 3, no. 4, pp. 395-410, Apr. 1959.

[14] R. E. Leadon, C. E. Mallon, and B. A. Green, "Dose and dose rate dependence of induced conductivity in dielectrics," *IEEE Trans. Nucl. Sci.,* vol. 20, no. 6, pp. 126-128, Dec. 1973.

[15] L. Weaver, J. K. Shultis, and R. E. Faw, "Analytic solutions of a model for radiation-induced conductivity in insulators," *J. Appl. Phys.,* vol. 48, no. 7, pp. 2762-2770, Jul. 1977.

[16] V. A. J. van Lint and J. W. Harrity, "Ionization radiation effects in insulators and insulating parts," *IEEE Trans. Elec. Insulat.,* vol. EI-6, no. 3, pp. 111-113, Sept. 1971.

[17] V. A. J. van Lint, J. W. Harrity, and T. M. Flanagan, "Scaling laws for ionization effects in insulators," *IEEE Trans. Nucl. Sci.,* vol. 15, no. 6, pp. 194-204, 1968.

[18] V. A. J. van Lint, T. M. Flanagan, R. E. Leadon, and J. A. Naber, *Mechanisms of radiation effects in electronic materials. Vol. 1*. New York: John Wiley & Sons, 1980.

[19] R. H. Bube, *Photoconductivity of solids*. New York: John Wiley & Sons, 1960.

[20] J. Mort and D. M. Pai, *Photoconductivity and related phenomena*: Elsevier Scientific Pub. Co., 1976.
[21] (2012, DuPont™ Pyralux® LF Sheet Adhesive. Available: http://www2.dupont.com/Pyralux/en_US/assets/downloads/pdf/LFadhesive_H-73246.pdf
[22] E. F. Hartman, T. A. Zarick, T. J. Sheridan, E. F. Preston, and T. A. Stringer, "Measurements of prompt radiation induced conductivity of Kapton," Sandia National Laboratories, Albuquerque, NM, SAND Report SAND2010-7284, Oct. 2010.
[23] M. McLain, "Laser-based radiation-induced conductivity in Kapton polyimide dielectrics at high dose rates," Sandia National Laboratories, Albuquerque, NM, SAND Report SAND2012-1582, Mar. 2012.
[24] E. F. Hartman, T. A. Zarick, T. J. Sheridan, and T. A. Stringer, "Measurements of prompt radiation induced conductivity of Fiberglass," Sandia National Laboratories, Albuquerque, NM, SAND Report SAND2010-2080, Apr. 2010.
[25] E. F. Hartman, T. A. Zarick, T. J. Sheridan, and E. F. Preston, "Measurements of prompt radiation induced conductivity in Teflon (PTFE)," Sandia National Laboratories, Albuquerque, NM, SAND Report SAND2013-3714, May 2013.

DISTRIBUTION

1 E. Preston
ITT Exelis
5009 Centennial Blvd.
Colorado Springs, CO 80919

1	MS 1152	C. D. Turner	1352
1	MS 1152	K. Cartwright	1352
1	MS 1167	T. A. Zarick	1343
1	MS 1167	T. J. Sheridan	1343
1	MS 1167	E. F. Hartman	1343
1	MS 1167	M. L. McLain	1343
1	MS 1167	T. M. Flanagan	1343
1	MS 1167	G. S. Heffelfinger	1340
1	MS 1168	B. V. Oliver	1352
1	MS 1179	W. C. Fan	1341
1	MS 1179	H. P. Hjalmarson	1341
1	MS 1179	C. R. Drumm	1341
1	MS 1179	S. D. Pautz	1341
1	MS 1179	L. Lorence	1341
1	MS 0899	Technical Library	9536 (electronic copy)